Supplementary Data

Characterization of CeO_2 Nanoparticles

Brunauer–Emmet–Teller specific surface area and porosity

To characterize specific surface area of nanoceria, N_2 adsorption–desorption isotherms were obtained on a Quantachrome Nova 3000 BET specific surface area analyzer at liquid nitrogen temperature. The samples were degassed at 90°C for 1 h before the measurements were taken. The specific surface area and the pore size distribution were calculated by the Brunauer–Emmett–Teller (BET) and Barrett–Joyner–Halenda (BJH) models, respectively. Replicate measurements were performed ($n=2$), and were within 5% of each other. The results are presented in Supplementary Table S1.

Isoelectric point

Nanoceria isoelectric point (IEP) of 7.5 was taken from Fang *et al.*,[1] because we used the same batch of nanoceria in our study.

Phase composition (Raman spectroscopy)

To characterize the phase composition of nanoceria and the redox state of the nanoparticles in water, Raman spectra were measured on nanoceria slurries using a $40\times$ or $50\times$ objective at two excitation wavelengths of 532 and 325 nm, respectively (laser power = 25 and 20 mW, respectively). As compared with X-ray diffraction, Raman spectroscopy has given better sensitivity of nanoceria local structural properties.[2–4] Excitation at 532 nm, which has lower energy than the nanoceria band gap of Raman spectroscopy, provides information about the phase composition of the whole nanoparticle. The UV excitation produces the resonant Raman spectra of the near-surface region.[2]

As seen from Supplementary Figure S1, the Raman spectrum of nanoceria excited by a 532-nm laser is dominated by a peak at around 465 cm^{-1} due to the F_{2g} symmetrical stretching of oxygen sublattice in fluorite cubic structure.[3,4] An additional peak at 600 cm^{-1} is assigned to the structural disorder due to Ce^{3+} in octahedral coordination.[5] The observed significant increase in the relative intensity of the Ce^{3+} peak relative to the F_{2g} peak in the resonant Raman spectra suggests that the nanoparticles have a significant concentration of Ce^{3+}, which is accumulated in the nanoparticle shell.

Supplementary Table S1. Characterization of CeO_2 Nanoparticles

Lattice structure from Raman	*BET surface area, m^2/g*	*Pore volume, cm^3/g*	*Pore diameter, nm*	*IEP*
Phase cubic fluorite	101 ± 5	0.5	22.7	7.5

BET, Brunauer–Emmett–Teller; IEP, isoelectric point.

Surface analysis (X-ray photoelectron spectroscopy)

To characterize the purity of the nanoparticle surface and the oxidation state of cerium cations, we performed the X-ray photoelectron spectroscopy (XPS) analysis. The spectra were collected with a Perkin Elmer PHI 5500 instrument using monochromatic AlKα X-rays with pass energies of 17.6 eV at resolution of 0.9 eV at take-off angle of 45° at pressures of $<1\times10^{-9}$ Torr, calibrated using the Au($4f_{7/2}$) peak at 84.0 eV. Regional scans within from 10 to 50 eV window widths were collected at 0.1-eV steps. To curve fit the O 1s spectra, the Shirley function was used to subtract the background. The deconvolution kernel was a Gaussian-Lorentzian (10%) function. The peak position calibrated by assuming a BE of 285 eV for sp^3 peak of adventitious carbon. The sample for the XPS analysis was processed as a thin nanoparticulate layer deposited from an aqueous slurry on the XPS holder and dried in air. The XPS spectra were reproduced on two samples in terms of peak widths, shapes, and positions, as well as surface atomic concentrations, within the experimental error of the method.

The survey XPS scan detects only Ce, O, and adventitious C (Supplementary Fig. S2). The Ce 3d regional spectrum (Supplementary Fig. S3) consists of six peaks corresponding to three main pairs of $3d_{3/2}$–$3d_{5/2}$ spin-orbit doublets of Ce(IV) oxide.[6] In addition, it exhibits weak peak at 885.3 eV typical of the Ce 3d spectrum of Ce(III) oxide. This observation is in agreement with the Raman (Supplementary Fig. S1) and UV-Vis (Supplementary Fig. S4) result that nanoceria is partially reduced.

Lattice defects and optical band gap of nanoceria from UV-Vis absorption spectra

To evaluate optical band gap of nanoceria, which determine their semiconducting properties, we measured a UV-Vis absorption spectrum of a diluted nanoceria suspension in water using a Lambda-25 (PerkinElmer) spectrophotometer at the scan speed of 120 nm/min and a 1-nm slit. The spectrum was run immediately after sonicating the suspensions for 30 min, in a 1-cm quartz cuvette.

As seen from Supplementary Figure S4a, a steep increase in the UV-Vis absorption of nanoceria starts at $\sim$400 nm. This feature corresponds to the optical band gap of the nanoparticles.[7] The Tauc-Mott analysis[8,9] of this spectrum was used to determine the type and value of the optical gap of the nanoceria. As seen from Supplementary Figure S4b, the nanoparticles have direct and indirect band gaps of 3.3 and 2.4 eV, respectively. Both the values are much lower than the indirect band gap of 4 eV of stoichiometric CeO_2.[10] The red shift of the band gap is due to the presence of Ce^{3+} cations, suggesting their high concentration. Ce^{3+} ions present in nanoceria create a trap state of $\sim$3 eV above the CeO_2 valence band due to the Ce 5*d*–Ce 4*f* transition. High defectiveness of the nanoceria lattice is also manifested by a pronounced absorption tail at wavelengths longer than 400 nm (Supplementary Fig. S4a). An ideal semiconductor lacks states below the band gap.[7]

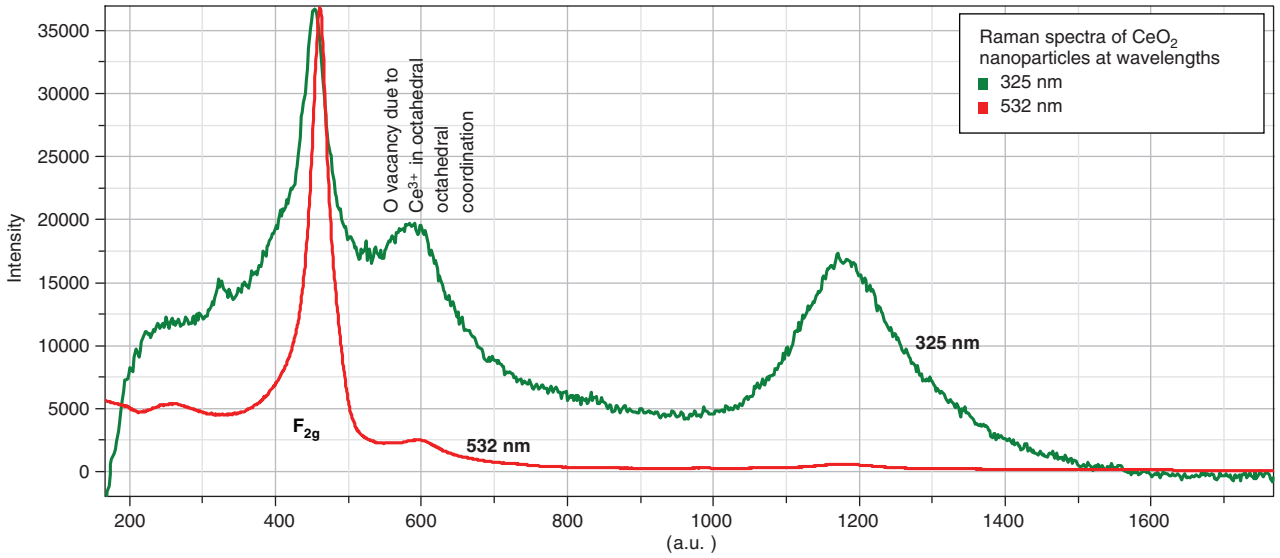

SUPPLEMENTARY FIG. S1. Raman spectra of nanoceria powder measured with (red) 532 nm and (green) 535 nm laser.

Processing of Raman spectra of individual chondrocytes

The optical image of cell 2 (Supplementary Fig. S8) slightly differs from the images of the cells shown in Figure 5 of the main article. Namely, the organelles and/or lipid bodies are concentrated in the center of cell 2, rather than being unevenly distributed. The Raman spectrum of this cell (Supplementary Fig. S9) exhibits, as compared with the average spectrum of five cells in the control, a significantly higher intensity of a peak at 1300 cm^{-1} due to the CH_2 twisting mode of hydrocarbon chains of saturated lipids. Moreover, it displays a pronounced peak at 1750 cm^{-1} due to the C=O stretching mode of ester group of lipids. Since no change in the choline peak at 710 cm^{-1} is observed, we conclude that cell 2 has a higher concentration of triacylglycerols. As noticed earlier,[11] the formation of lipid bodies can be induced by stress such as accidental inflammation or the measurement conditions.

Effect of Nanoceria on the Mechanical Properties and Raman Spectra: Repeat Experiments

To justify our protocol of Raman measurements, we verified whether the average Raman spectra of 4–6 randomly selected cells can represent the sample and is as valid as the average of more than 30 cells (Supplementary Figs. S10 and S11). For this purpose, we repeated Study 1 to investigate the effects of nanoceria at a concentration 1000 µg/mL, without IL-1α. We followed the same protocols for construct preparation and for measuring Raman spectra as reported in the main text. Briefly, Raman spectra were measured in two ranges of 300–1200 and 1180–1800 cm^{-1} on individual living chondrocytes in ~1-mm-sliced sections of constructs immersed in phosphate-buffered saline. We acquired spectra of 30–35 cells for both nanoceria and control sets. Each spectra was measured for 5 min with no attenuation of the laser source.

The Raman spectrum of the nanoceria construct averaged over 32 cells shows increased concentrations of procollagen, glycogen, and proteoglycans as compared with the control sample averaged over 35 cells (Supplementary Fig. S10). The same trend is reproduced in the average of five cells from each sample (Supplementary Fig. S11). Both these trends correlate with the increased mechanical strength of the nanoceria scaffold (Fig. 3). These results demonstrate that our Raman results averaged with five to six cells can be used for the purpose of our study (Fig. 6).

Supplementary References

1. Fang, X.H., Li, B.Q., Chernyshova, I.V., and Somasundaran, P. Ranking of as-received micro/nanoparticles by their surface energy values at ambient conditions. J Phys Chem C **114,** 15473, 2010.
2. Guo, M., Lu, J.Q., Wu, Y.N., Wang, Y.J., and Luo, M.F. UV and Visible Raman studies of oxygen vacancies in rare-earth-doped Ceria. Langmuir **27,** 3872, 2011.
3. Spanier, J.E., Robinson, R.D., Zheng, F., Chan, S.W., and Herman, I.P. Size-dependent properties of CeO2-y nanoparticles as studied by Raman scattering. Phys Rev B **64,** 245407, 2001.
4. Zhang, F., Chan, S.W., Spanier, J.E., Apak, E., Jin, Q., Robinson, R.D., *et al.* cerium oxide nanoparticles: size-selective formation and structure analysis. Appl Phys Lett **80,** 127, 2002.
5. Taniguchi, T., Watanabe, T., Sugiyama, N., Subramani, A.K., Wagata, H., Matsushita, N., *et al.* Identifying defects in Ceria-based nanocrystals by UV resonance Raman spectroscopy. J Phys Chem C **113,** 19789, 2009.
6. Matolin, V., Matolinova, I., Sedlacek, L., Prince, K.C., and Skala, T. A resonant photoemission applied to cerium oxide based nanocrystals. Nanotechnology **20,** 215706, 2009.
7. Pankove, J.I. Optical Processes in Semiconductors. New York: Dover Publications, Inc., 1971.
8. Mott, N.F., and Davis, E.A. Electronic Processes in Non-crystalline Materials. Oxford: Clarendon, 1979.
9. Tauc, J. Optical Properties of Solids. New York: Plenum, 1969.
10. Patsalas, P., Logothetidis, S., Sygellou, L., and Kennou, S. Structure-dependent electronic properties of nanocrystalline cerium oxide films. Phys Rev B **68,** 035104, 2003.
11. Zoladek, A., Pascut, F.C., Patel, P., and Notingher, I. Non-invasive time-course imaging of apoptotic cells by confocal Raman micro-spectroscopy. J Raman Spectrosc **42,** 251, 2011.

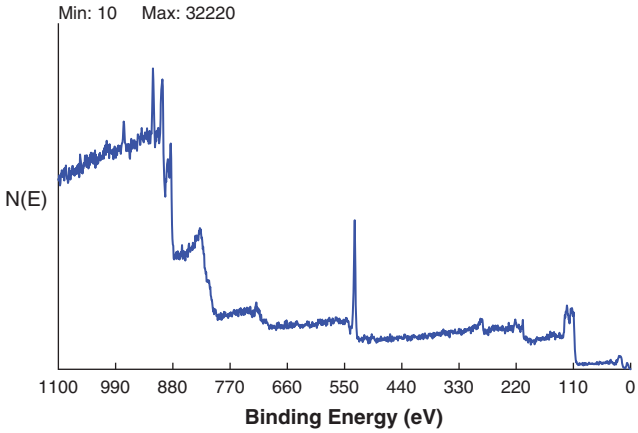

SUPPLEMENTARY FIG. S2. Survey X-ray photoelectron spectrum of CeO_2 nanoparticles.

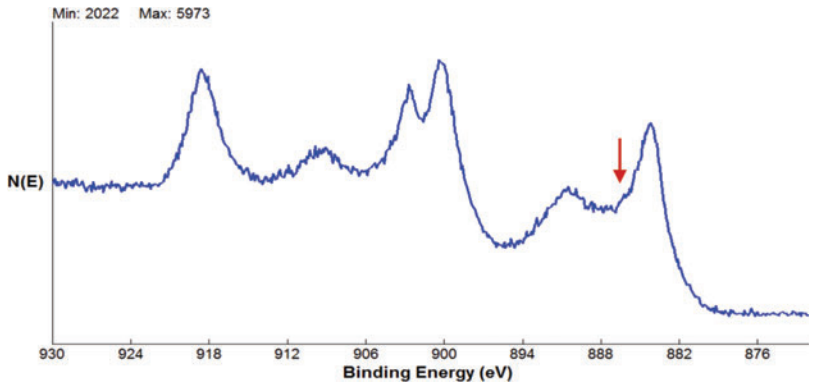

SUPPLEMENTARY FIG. S3. The Ce 3d core-level photoemission spectrum of CeO_2 nanoparticles. Arrow indicates a shoulder due to Ce^{3+}.

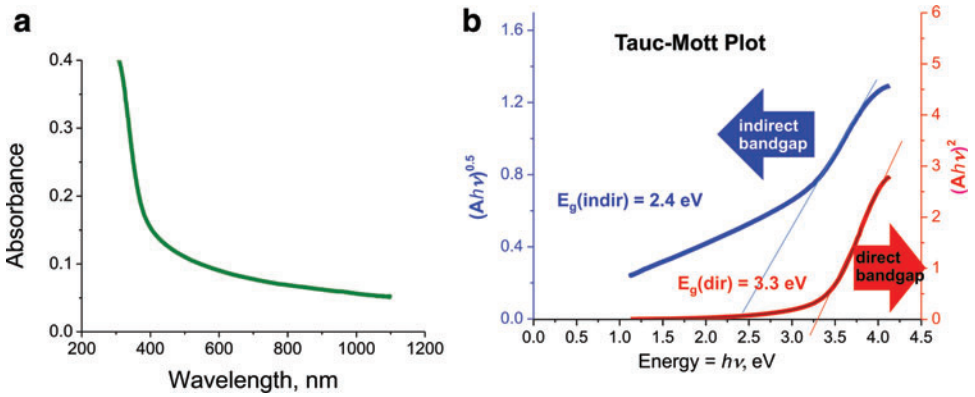

SUPPLEMENTARY FIG. S4. **(a)** UV-Vis absorption spectrum of a nanoceria aqueous suspension and **(b)** derived Tauc-Mott plot.

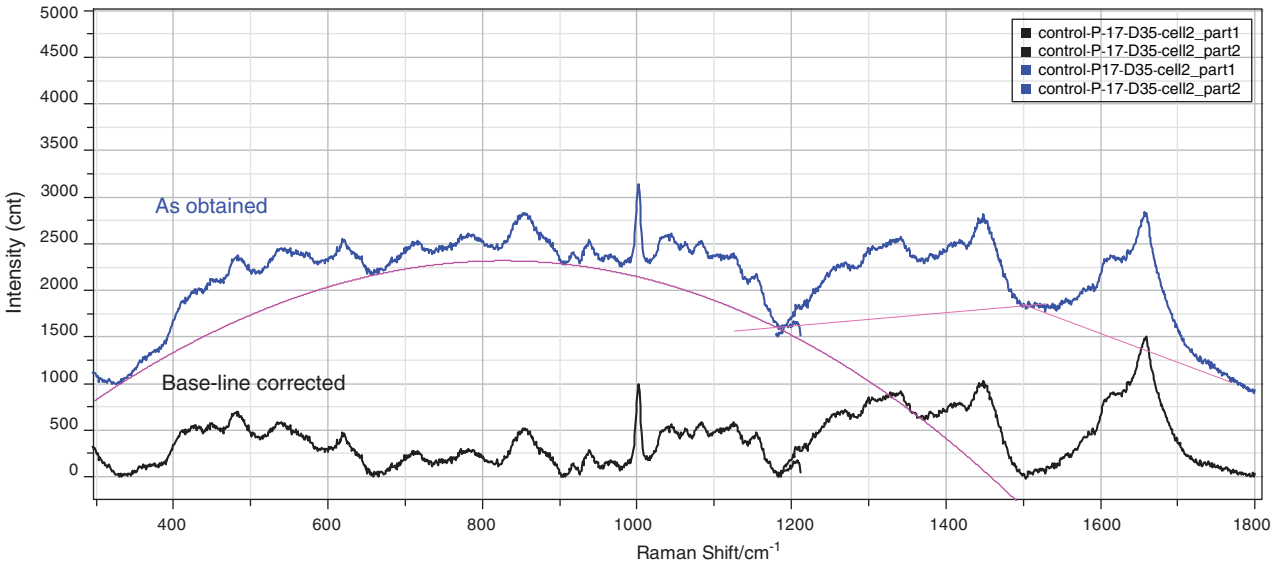

SUPPLEMENTARY FIG. S5. Illustration of baseline correction in two spectral regions measured for spectra on cell No. 2 of the control sample.

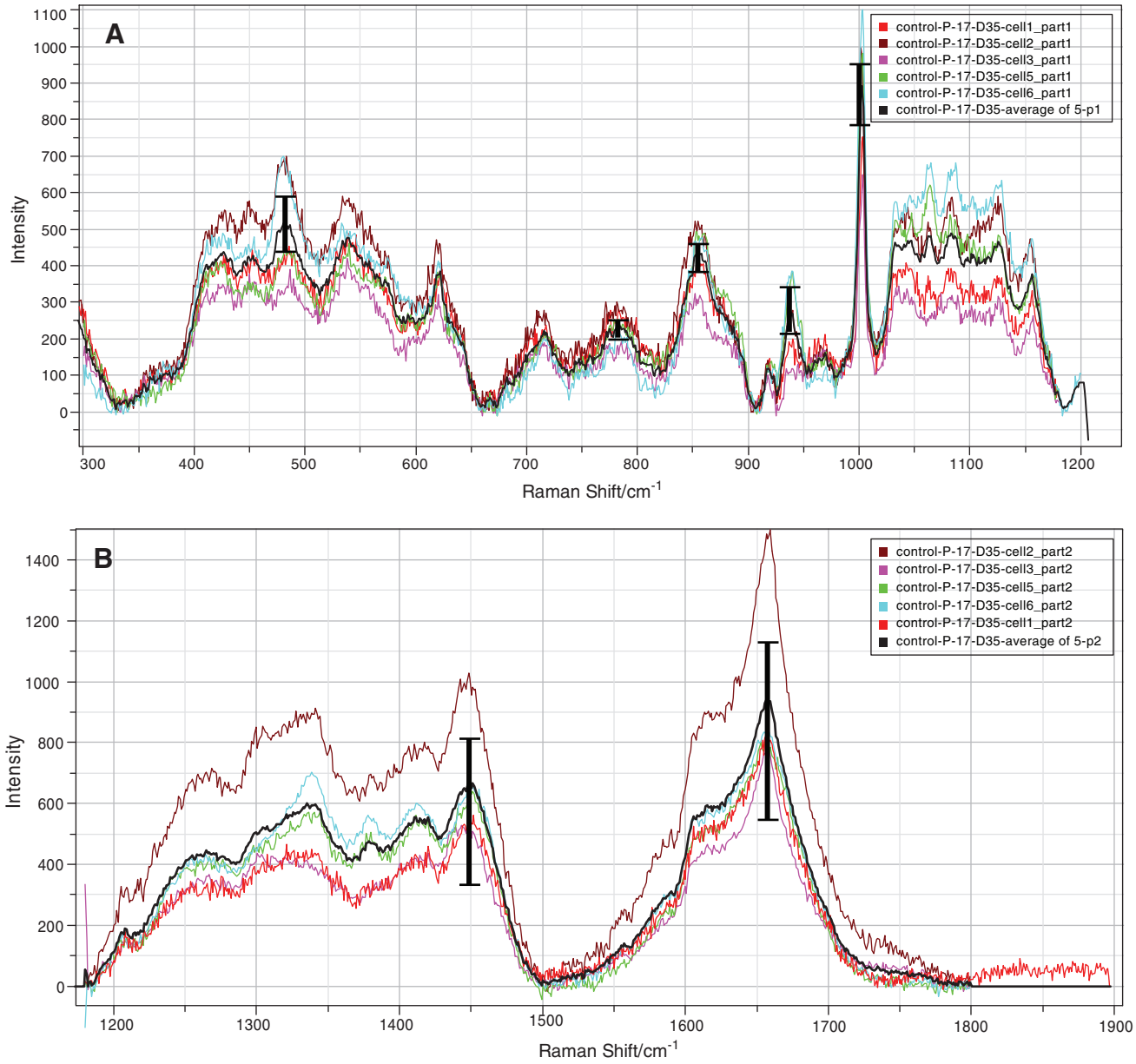

SUPPLEMENTARY FIG. S6. Statistical analysis of the Raman spectra of five individual cells of the control sample in two spectral regions analyzed: **(A)** 300–1200 and **(B)** 1200–1900 cm^{-1}. The average spectrum and the standard deviation are shown in black.

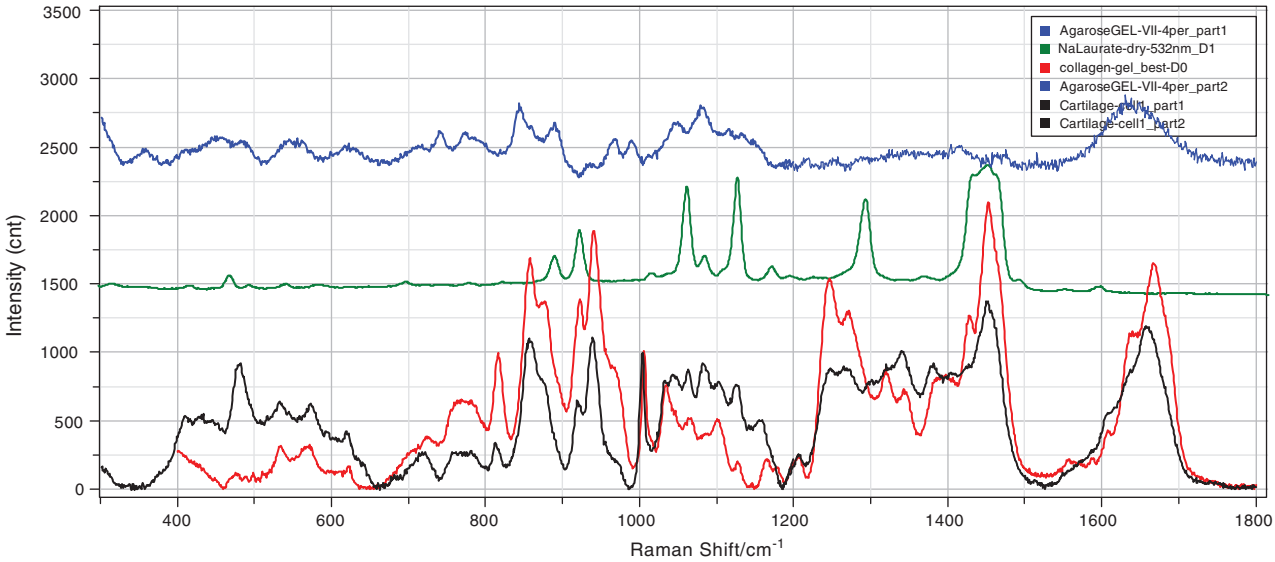

SUPPLEMENTARY FIG. S7. Raman spectra of (black) a chondrocyte of bovine cartilage, (red) collagen type II from chicken sternal cartilage (Sigma), (blue) agarose gel, and (green) solid fatty acid (sodium laurate). Collagen was prepared as a transparent gel by mixing of the equal weights of water and a dry collagen powder.

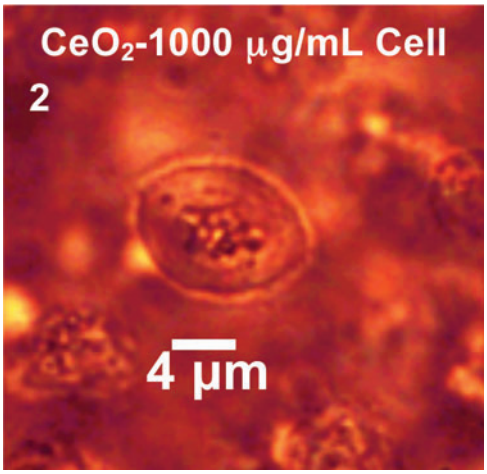

SUPPLEMENTARY FIG. S8. Optical image of cell No. 2 from the six-cell set from the scaffold loaded with 1000 μg/mL of nanoceria.

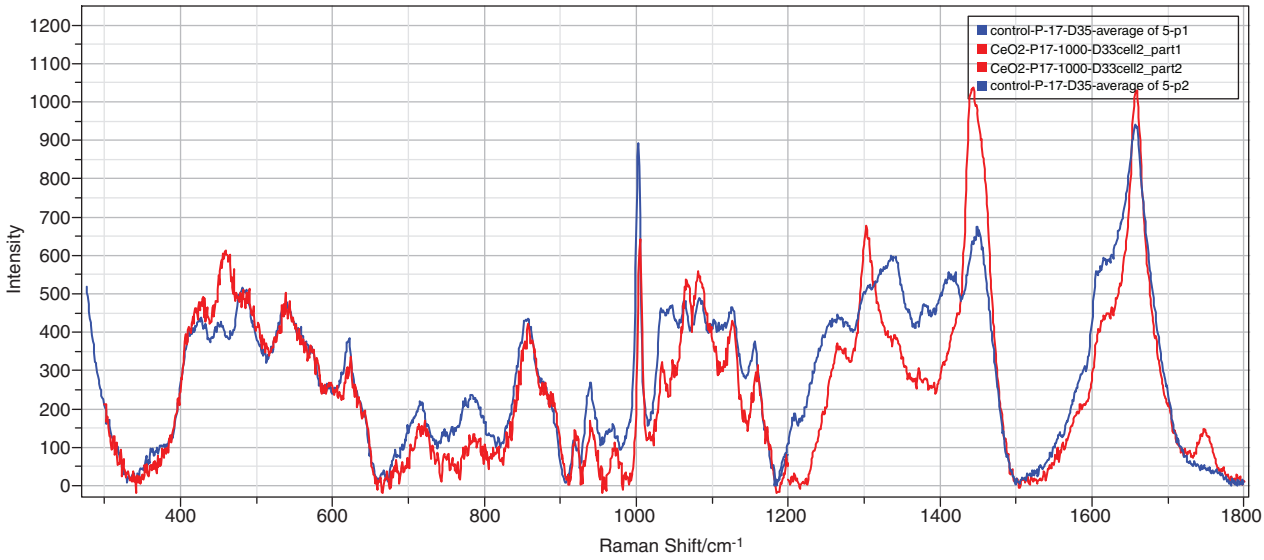

SUPPLEMENTARY FIG. S9. Raman spectra of (blue) average spectrum of five control cells and (red) cell No. 2 from the scaffold embedded with 1000 μg/mL of nanoceria in Study 1. See text for more detail.

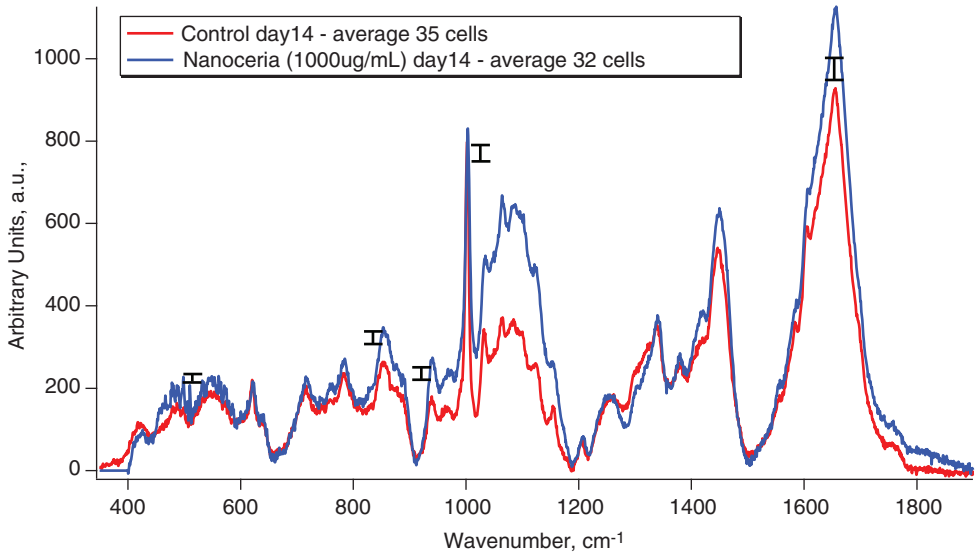

SUPPLEMENTARY FIG. S10. Raman spectra of (blue) 32 individual chondrocytes in a scaffold embedded with 1000 μg/mL nanoceria acquired at day 14 in comparison with (red) an average spectrum of 35 control cells. Vertical bars show standard deviations in the main diagnostic peaks (Table 1) for the average spectrum of the control sample.

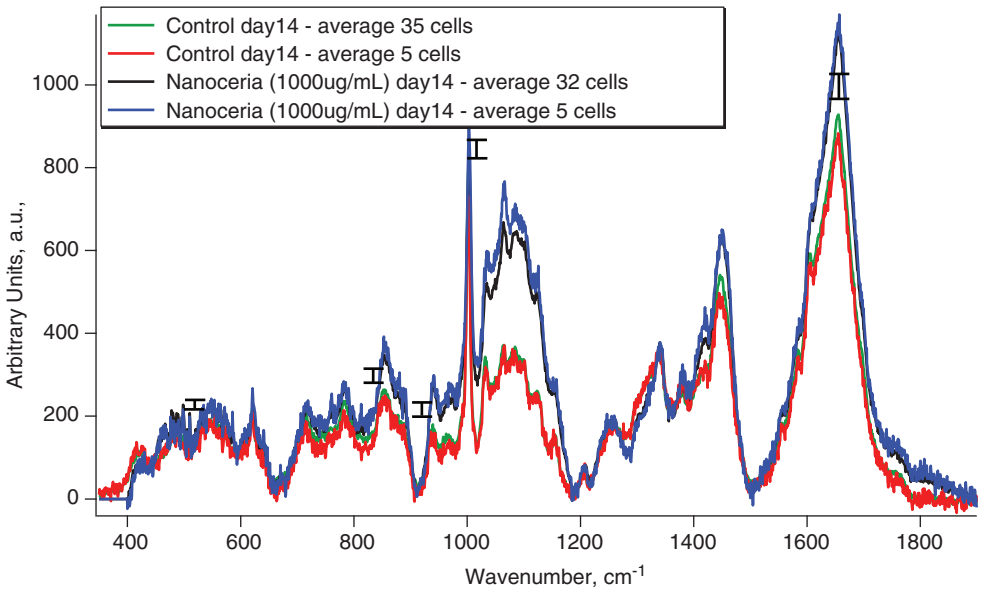

SUPPLEMENTARY FIG. S11. A comparison of Raman spectra of 5 (blue) and 32 (black) individual chondrocytes in a scaffold embedded with 1000 μg/mL nanoceria. A similar comparison for control of spectra is shown for 5 cells (red) and 35 cells (green). Vertical bars show standard deviations in the main diagnostic peaks (Table 1) for the average spectrum of the control sample.